Available online at www.sciencedirect.com

ScienceDirect

Procedia Structural Integrity 37 (2022) 865–872

Structural Integrity Procedia

www.elsevier.com/locate/procedia

ICSI 2021 The 4th International Conference on Structural Integrity

Combined approach for fatigue crack characterisation in metals

J. M. Robles[1], J. M. Vasco-Olmo[2], A. S. Cruces[1], F. A. Diaz[2], M. N. James[3, 4], P. Lopez-Crespo[1]

[1] *Department of Civil and Materials Engineering, University of Malaga, C/Dr Ortiz Ramos, s/n, 29071 Malaga, Spain*
[2] *Universidad de Jaén , Departamento de Ingeniería Mecánica y Minera, Escuela Politécnica Superior de Jaén, Ronda Sur, S/N, 23700 Linares, Jaén*
[3] *University of Plymouth, School of Marine Science & Engineering, Drake Circus, PL4 8AA, Plymouth, United Kingdom*
[4] Nelson Mandela Metropolitan University, Department of Mechanical Engineering, PO Box 77000, 6031, Port Elizabeth, South Africa
[b] *Second affiliation, Address, City and Postcode, Country*

Abstract

In this work a comprehensive characterisation of the fatigue crack growth of an Al 2024 alloy is presented. A powerful Christopher-James-Patterson (CJP) model is used for multi-parameter characterisation of the crack state at a few different locations through the fatigue crack growth. The CJP model of crack tip displacements and stress fields was proposed in order to better capture the influences on the applied elastic stress field of the plastic enclave that is generated around a growing fatigue crack. The model does this through a set of elastic stresses applied at a notional elastic-plastic boundary, and it has been shown to accurately model plastic zone shape and size, whilst its ability to predict the effective range of stress intensity factor during a fatigue cycle has been verified. Thus, the model can predict the driving force component of the crack and additional components that account for different shielding mechanisms. CJP model is combined with full-field non-contact Digital Image Correlation (DIC) so that the model can be fed at any moment with real experimental information. The results are then correlated with Paris law data for Al 2024 alloy through Scanning Electron Microscopy (SEM) observations of the fracture surface. In this work the effect of crack length and load level are thoroughly studied and validated with fatigue crack growth rate measurements.

Keywords: Fatigue crack growth; Digital Image Correlation; SEM; CJP model

10.1016/j.prostr.2022.02.020

1. Introduction

In modern industry, fatigue failure is still the main cause of machine element failure. Some industries are particularly affected by this type of failure, such as the aeronautical industry. For this reason, and for both economic and safety reasons, it is necessary to develop more complex models that predict fatigue failure more accurately, with those based on the effect of the plastic zone on crack growth currently deserving special attention (Pablo Lopez-Crespo and Pommier 2008).

Crack growth analysis has been studied for several years. The Paris law (Paris, P., Erdogan 1963) was the support on which many studies have been based. However, the models must become more complex to incorporate the number of effects and parameters that the Paris law does not take into account, such as the effect of the thickness of the specimen (Bao and McEvily 1998), the stress ratio, which was attempted to be included by equations such as that of Forman (Forman, Kearney, and Engle 1967) and Walker (Walker 1970). In addition, of course, to explain the effect of both tensile and compressive overloads, more advanced models are needed and the concept of the phenomenon of plasticity crack closure must be introduced (Elber W 1970). With these considerations, some of the effects that produce the acceleration or retardation of crack growth could be explained (Fellows and Nowell 2005)(P. Lopez-Crespo et al. 2015). However, there is debate about the real effect on propagation (Sadananda et al. 1999) and also about the best way to measure the crack closure effect (Xia, Kujawski, and Ellyin 1996)(Stoychev and Kujawski 2003).

In this context, new models emerge to try to approximate more accurately the fatigue crack growth and, therefore, the fatigue life of the material. One of these models will be studied in this work, the Christopher, James, Patterson model (CJP model) (Christopher et al. 2007). This model is based on William's equation, complemented with the influence of the plastic zone in the elastic-plastic boundary and developed from the method of Muskhelishvili's (Muskhelishvili NI 1977) complex potentials (James, Christopher, Lu, Tee, et al. 2011). With the application of this method, four parameters of interest for fatigue studies are obtained: the open mode stress intensity factor (K_f), the retardation stress intensity factor (K_r), the shear stress intensity factor (K_s) and the T-stress (Olmo et al. 2011)(James, Christopher, Lu, and Patterson 2011). Using this model, several studies have shown that it gives good results when the plasticity play an important role (Vasco-Olmo, Díaz, and Patterson 2016) and that it is able to capture the perturbations produced by the effect of local plastic deformations (James et al. 2013). Vasco-Olmo also demonstrated that the size and shape of the plastic zone can be approximated more accurately with this method than with other traditionally used methods (Vasco-Olmo et al. 2016).

In order to check if crack growth is accurately predicted using this model, the theoretical data provided by the CJP model will be supported with experimental data obtained by SEM observation. For this study the fracture surface will be observed for fatigue marks, by measuring the distance between them the parameter da/dN could be obtained (Forsyth and Ryder 1960).

2. CJP model

The CJP model is used in the current work to characterise crack tip fields. It is a novel mathematical model developed by Christopher, James and Patterson (James et al. 2013). The authors postulated that the plastic enclave which exits around the tip of a fatigue crack and along its flanks will shield the crack from the full influence of the applied elastic stress field and that crack tip shielding includes the effect of crack flank contact forces (so-called crack closure) as well as a compatibility-induced interfacial shear stress at the elastic-plastic boundary.

Crack tip displacement fields (James et al. 2013) were characterised as:

$$\begin{aligned} 2G(u+iv) = \kappa & \left[-2(B+2E)z^{\frac{1}{2}} + 4Ez^{\frac{1}{2}} - 2Ez^{\frac{1}{2}}\ln(z) - \frac{C-F}{4}z\right] \\ & - z\left[-(B+2E)\bar{z}^{\frac{1}{2}} - E\bar{z}^{\frac{1}{2}}\overline{\ln(z)} - \frac{(C-F)}{4}\right] \\ & - \left[A\bar{z}^{\frac{1}{2}} + D\bar{z}^{\frac{1}{2}}\overline{\ln(z)} - 2D\bar{z}^{\frac{1}{2}} + \frac{C+F}{2}\bar{z}\right] \end{aligned} \quad (1)$$

Where G is the shear modulus, $\kappa=(3-\nu)/(1+\nu)$ for plane stress or $\kappa=3-4\nu$ for plane strain, where ν is the Poisson's

ratio of the material and A, B, C, D, E and F are the coefficients that define crack tip displacement fields in the model.

The opening mode stress intensity factor K_F is defined using the applied remote load traditionally characterised by K_I but that is modified by force components derived from the stresses acting across the elastic-plastic boundary and which therefore influence the driving force for crack growth.

$$K_F = \lim_{r\to 0}\left[\sqrt{2\pi r}\left(\sigma_y + 2Er^{\left(-\frac{1}{2}\right)}\ln(r)\right)\right] = \sqrt{\frac{\pi}{2}}(A - 3B - 8E) \tag{2}$$

The retardation stress intensity factor K_R characterises forces applied in the plane of the crack and which provide a retarding effect on fatigue crack growth. Thus, K_R is evaluated from σ_x in the limit as $x \to$ -0, along $y = 0$, i.e. towards the crack tip along the crack flank:

$$\begin{aligned} K_R &= \lim_{r\to 0}[\sqrt{2\pi r}\,\sigma_x] \\ &= -(2\pi)^{\frac{3}{2}}E \end{aligned} \tag{3}$$

The shear stress intensity factor K_S characterises compatibility-induced shear stress along the plane of the crack at the interface between the plastic enclave and the surrounding elastic field and is derived from the asymptotic limit of σ_{xy} as $x \to$ -0, along y = 0, i.e. towards the crack tip along the crack wake:

$$\begin{aligned} K_S &= \lim_{r\to 0}[\sqrt{2\pi r}\,\sigma_{xy}] \\ &= \pm\sqrt{\frac{\pi}{2}}(A + B) \end{aligned} \tag{4}$$

A positive sign indicates $y > 0$, and a negative sign that $y < 0$.

The T-stress, which is found as components T_x in the x-direction and T_y in the y-direction is given by:

$$\begin{aligned} T_x &= -C \\ T_y &= -F \end{aligned} \tag{5}$$

3. Material and methods

3.1. Material

The material used in this work is the aluminium alloy 2024. This alloy is usually formed by precipitation, with the combination of the S-phase (Al2CuMg), the Guinier Preston Bagaryatsky zones and other different precipitate groups playing an important role (Sha et al. 2011). Table 1 shows the mechanical properties of this alloy according to the ASM HandBook - Volume 02 (ASM Metals Handbook - Properties and selection nonferrous alloys and special purpose- Volume 2 1996):

Table 1. Mechanical properties Al2024 alloy.

Ultimate tensile strength (MPa)	Tensile yield strength (*MPa*)	Elongation in 50mm (%)	Hardness Brinell (HB)	Ultimate shearing strength (MPa)	Fatigue endurance limit (MPa)	Modulus of elasticity (GPa)	Modulus of Poisson
485	345	18	120	285	140	73	0.33

In order to study the grain size it is necessary reveal the microstructure of the material. Figure 1 shows the material after revealing the microstructure, for this, first, a polishing process divided into 4 stages was carried out, reducing the

size of the abrasive in each stage. The equipment use to make the grinding and the polishing was Struers-TegraPol11. After polishing, a Keller etching was performed with the compositions indicated in ASM Metals Handbook - Volume 9 (ASM Metals Handbook -Metallography and Microstructures, Volume 9 2004).

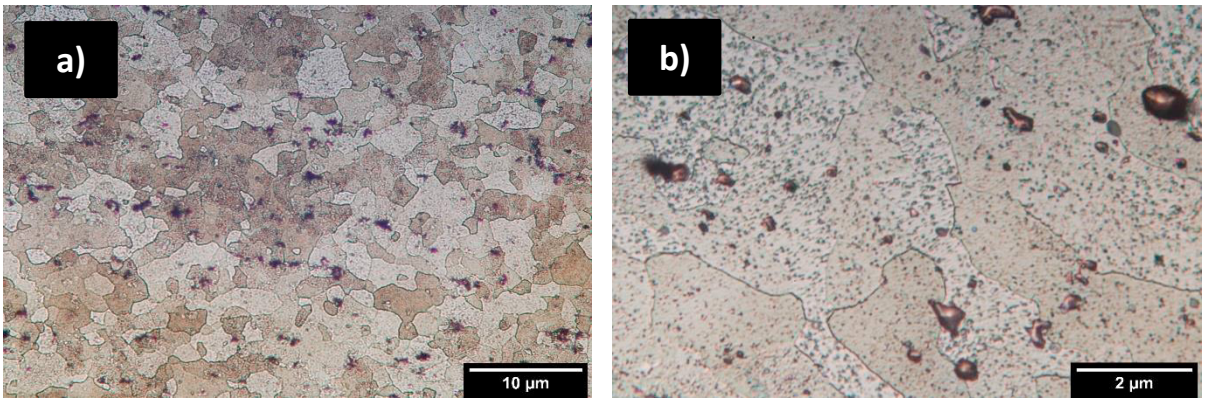

Figure 1. Microestructura a) Al 2024 x200. b) Al 2024 x1000.

The intercept method was used to calculate the grain size of the material to both samples which is explained in ASTM-E112 (ASTM-E112: Standard Test Methods for Determining Average Grain Size 2010). In order to reduce the variance of the data, this process was applied in nine areas of each sample to calculate the mean value. After the application of this, the average grain size for AL20214-CT3 is 2.8µm and in the sample AL2024-CT5 is 3.05µm, this values are close enough to assume a similar fatigue behaviour.

3.2. SEM procedure

For the purpose of characterising the crack growth through SEM observations the next procedure was developed:

- First step is correct colocation of the sample, in this case the specimen was positioned to match the X-axis of the microscope with the crack growth direction with the intention of obtained the crack length directly.
- When a zone where there are fatigue marks are located, the next step is make a gradual approach to the interest area. The figure 2 show the fatigue marks clearly, it is important approach until the distance between the different marks could be measured accurately.
- Then, the distance between fatigue marks must be measure, in this case the software used for this task was ImageJ. Due to the scattering of the measures, the largest number of measurements should be made in each zone. In order to estimate the da/dN parameter in this area the average of all the distances is calculated.
- Finally to represent the curves da/dN-ΔK, the stress intensity factor range must be calculated with the standard ASTM-E1820.

Thus, as the crack progresses, a logarithmic relationship between the parameter da/dN and ΔK can be observed, as was seen in Hertzberg's studies (Hertzberg and Euw 1973). Another interesting fact that can be obtained by observing the fatigue marks is that the depth of the marks is closely related to the intensity of the load (Fleck and Smith 1981). Some studies (Chernyatin et al. 2018) shows the good correlation between the curves obtained with the Nasgro (Moreno et al. 2015) and the data obtained by SEM observation.

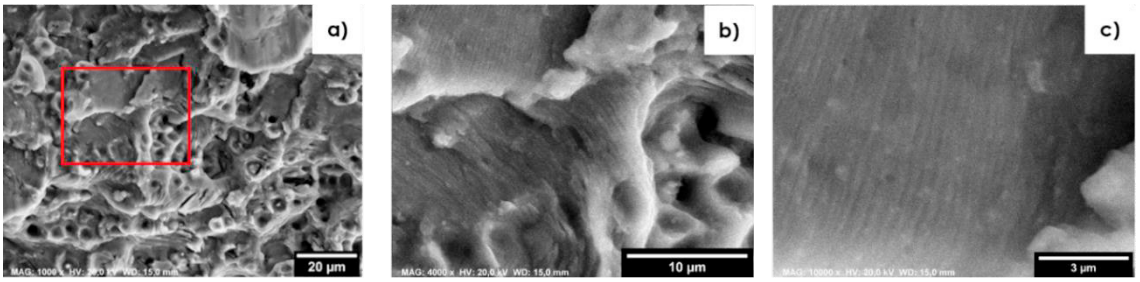

Figure 2. a) Fracture surface AL2024-CT3 X1000. b) Fracture surface AL2024-CT3 X4000. c) Fracture surface AL2024-CT3 X10000.

3.3. Testing details

Two CT specimens (dimensions shown in Figure 3a) were manufactured from a 2 mm thick sheet of 2024-T3 aluminium alloy and tested at constant amplitude loading at two different stress ratio values (R = 0 and 0.5). The loading cycle applied on the specimen tested at low stress ratio was between 5 N and 600 N, while that cycle applied on the specimen tested at high stress ratio was between 600 N and 1200 N.

The surface used for the DIC study was sprayed with a random black speckle pattern over a white background, while the other surface of the specimen was ground and polished to allow tracking of the crack tip position.

Fatigue tests were conducted on a MTS 370.10 servohydraulic machine (Figure 3b) with a loading capacity of 100 kN at a loading frequency of 10 Hz. A CCD camera, fitted with a 75 mm lens was placed perpendicularly to each face of the specimen. For determining stress intensity factor, the multi-point over-deterministic method developed by Sanford and Dally (Sanford and Dally 1979) forms the basis of this process.

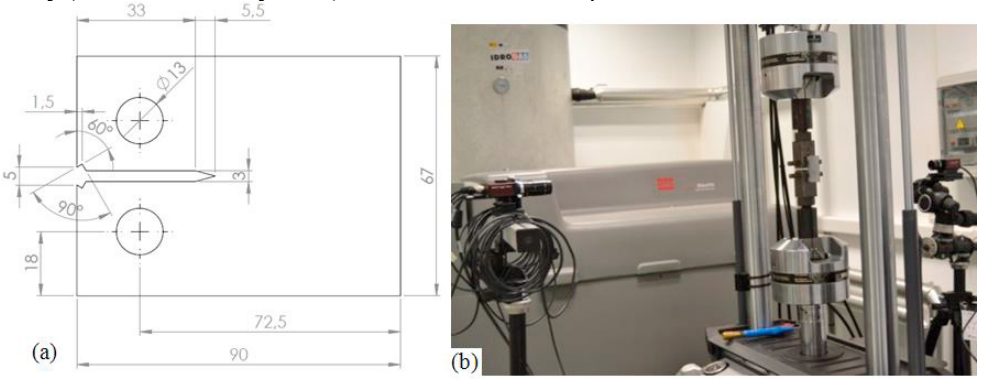

Figure 3. CT specimen (a) and experimental set-up for fatigue testing and data acquisition (b).

An annular mesh (Figure 4) was therefore defined with an inner radius large enough to avoid including plastic deformation at the crack tip and an outer radius that lies within the region dominated by the elastic stress singularity.

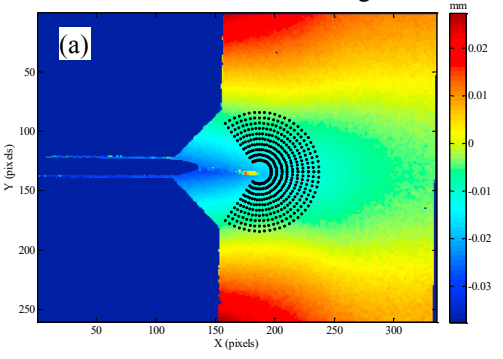

Figure 4. Horizontal displacement fields at a crack length of 34.10 mm and a load level of 600 N and data point collection.

4. Results

4.1. SEM results

The main parameter calculate through SEM observation is da/dN, for the purpose of obtaining a significant characterization more than fourteen areas for each sample are observed. The evolution of the parameter *da/dN* in front of the crack length (*a*) is represent on the figure 5.

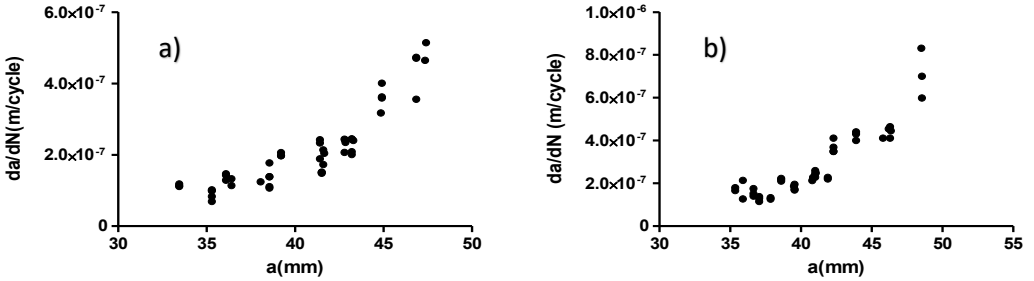

Figure 5. Evolution of the parameter da/dN in front of a: a) AL2024-CT3, b)AL2024-CT5

The comparison of both crack growth samples curves represent on the figure 6, in which SIF nominal values are considered, show the effect of the stress ratio due to the different test conditions. The SIF range is the same in both specimens, however, the stress ratio and the K_{max} is higher on AL2024-CT5. This characteristics produce that AL2024-CT5 curve has a displacement on the left, which represent a faster growth. For the purpose of calculating the effective SIF, the opening load must be measure. Vasco-Olmo (Olmo 2014) calculate this value and the evolution of this can be seen in the figure 7.

Figure 6 present the nominal results when applied the equations for compact tension (CT) of the ASTM-E1820 (ASTM-E1820: Standard Test Method for Measurement of Fracture Toughness 2001). With the objective of calculating the effective SIF range, the equation must change and use the opening load instead of the minimum load.

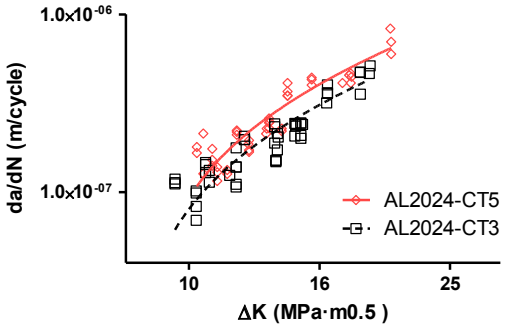

Figure 6. AL2024-CT3 and AL2024-CT5 da/dN in front of SIF nominal range

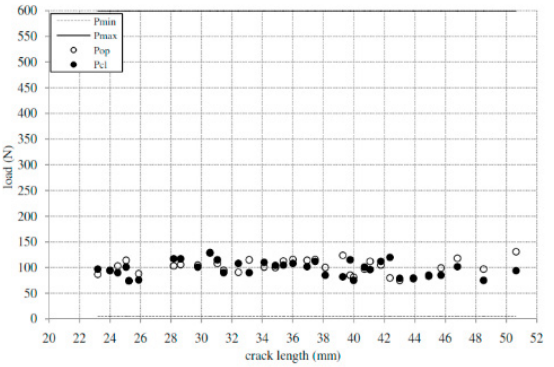

Figure 7. Evolution of the opening load and closure load during the test

4.2. CJP and SEM combined results

In order to obtain a combined approach of the crack growth the experimental data obtained from SEM analysis and theoretical data obtained from the application of the CJP model must be considered. The approach was made for the

sample AL2024-CT3, this sample present crack closure effect, in this way there is a significant different between nominal SIF range and effective SIF range. The figure 8 show the crack growth rate in front of SIF range for three different approach, the CJP approach, SEM effective SIF range and SEM nominal SIF range.

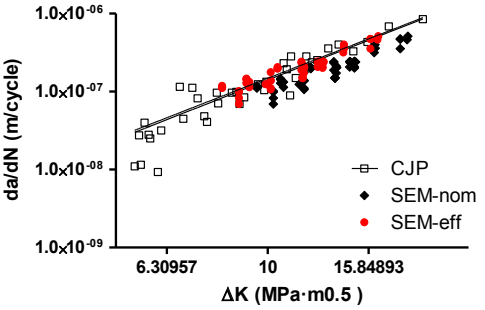

Figure 8. CJP, SEM effective SIF range and SEM nominal SIF range characterisation of crack growth

Moreover, figure 8 include a non-linear regression of the CJP curve on the zone where the crack growth rate have a constant increase. In this way was possible approximate the curve to the Paris law equation, which is shown on the equation 6.

$$\frac{da}{dN} = C \cdot \Delta K^m \tag{6}$$

Through the non-linear regression the parameters C and m are obtained, the value of C is $4.3 \cdot 10^{-10}$ and m is 2.529, the parameter of correlation R^2 for this approach is 0.948.

5. Conclusions

For this sample of aluminium 2024 alloy, the following conclusions can be deduced:

- The combined approach of the crack growth show that the data obtained from CJP are close to experimental data obtained from SEM in the case of the effective SIF range.
- Further analysis of SEM data showed that the distance measure between marks for a<36mm provide reliable results.
- Obtained results suggest that CJP model have potential to characterise fatigue behaviour even when crack closure effect is presented.

References

ASM Metals Handbook - Properties and Selection Nonferrous Alloys and Special Purpose- Volume 2. 1996.

ASM Metals Handbook -Metallography and Microstructures, Volume 9. 2004. ASM Metals Handbook.

"ASTM-E112: Standard Test Methods for Determining Average Grain Size." 2010. : 1–27.

"ASTM-E1820: Standard Test Method for Measurement of Fracture Toughness." 2001. : 1–46.

Bao, H., and A. J. McEvily. 1998. "On Plane Stress-Plane Strain Interactions in Fatigue Crack Growth." *International Journal of Fatigue* 20(6): 441–48.

Chernyatin, A. S., P. Lopez-Crespo, B. Moreno, and Yu G. Matvienko. 2018. "Multi-Approach Study of Crack-Tip Mechanics on Aluminium 2024 Alloy." *Theoretical and Applied Fracture Mechanics* 98(September): 38–47.

Christopher, C. J., M. N. James, E. A. Patterson, and K. F. Tee. 2007. "Towards a New Model of Crack Tip Stress Fields." *International Journal of Fracture* 148(4): 361–71.

Elber W. 1970. "Fatigue Crack Closure Under Cyclic Tension." *Engineering Fracture Mechanics* 2(1): 37–44.

Fellows, L. J., and D. Nowell. 2005. "Measurement of Crack Closure after the Application of an Overload Cycle, Using Moiré Interferometry."

International Journal of Fatigue 27(10–12): 1453–62.

Fleck, N. A., and R. A. Smith. 1981. "Effect of Density on Tensile Strength, Fracture Toughness, and Fatigue Crack Propagation Behaviour of Sintered Steel." *Powder Metallurgy* 24(3): 121–25.

Forman, R. G., V. E. Kearney, and R. M. Engle. 1967. "Numerical Analysis of Crack Propagation in Cyclic-Loaded Structures." *Journal of Basic Engineering* 89: 459–63.

Forsyth, P. J. E., and D. A. Ryder. 1960. "Fatigue Fracture, Some Results Derived from the Microscopic Examination of Crack Surfaces." *Aircraft Engineering* 32: 96–99.

Hertzberg, Richard W., and Eric F. J. Von Euw. 1973. "Crack Closure and Fatigue Striations in 2024-T3 Aluminum Alloy." 4: 887–89.

James, M. N., C. J. Christopher, Yanwei Lu, K. F. Tee, et al. 2011. "Crack Tip Shielding from a Plastic 'Inclusion.'" *Key Engineering Materials* 465: 1–8.

James, M. N., C. J. Christopher, Yanwei Lu, and E. A. Patterson. 2013. "Local Crack Plasticity and Its Influences on the Global Elastic Stress Field." *International Journal of Fatigue* 46: 4–15.

James, M N, C J Christopher, Yanwei Lu, and E A Patterson. 2011. "The Plastic inclusion as a Bridge between Local Crack Plasticity and the Global Elastic Field." *First IJFatigue & FFEMS Joint Workshop*: 178–84.

Lopez-Crespo, P. et al. 2015. "Measuring Overload Effects during Fatigue Crack Growth in Bainitic Steel by Synchrotron X-Ray Diffraction." *International Journal of Fatigue* 71: 11–16.

Lopez-Crespo, Pablo, and Sylvie Pommier. 2008. "Numerical Analysis of Crack Tip Plasticity and History Effects under Mixed Mode Conditions." *Journal of Solid Mechanics and Materials Engineering* 2(12): 1567–76.

Moreno, B. et al. 2015. "On the Use of NASGRO Software to Estimate Fatigue Crack Growth under Variable Amplitude Loading in Aluminium Alloy 2024-T351." *Procedia Engineering* 101(C): 302–11.

Muskhelishvili NI. 1977. *Some Basic Problems of the Mathematical Theory of Elasticity.* Groningen: Noordhoff International Publishing.

Olmo, J.M. Vasco. 2014. "Experimental Evaluation of Plasticity Induced Crack Shielding Effect Using Full-Field Optical Techniques for Stress and Strain Measurement PhD Student :" Universidad de Jaén.

Olmo, J.M. Vasco, F. A. Díaz Garrido, R. Dorado Vicente, and R. López García. 2011. "Comparativa de Modelos Para El Cálculo Experimental Del Factor de Intensificación de Tensiones Empleando Técnicas Ópticas de Campo Completo." *Asociación Española de Ingeniería Mecánica*.

Paris, P., Erdogan, F. 1963. "A Critical Analysis of Crack Propagation Laws." *J. Basic Eng* 85: 528–33.

Sadananda, K., A. K. Vasudevan, R. L. Holtz, and E. U. Lee. 1999. "Analysis of Overload Effects and Related Phenomena." *International Journal of Fatigue* 21(1): 233–46.

Sanford, Robert J., and James W. Dally. 1979. "A General Method for Determining Mixed-Mode Stress Intensity Factors from Isochromatic Fringe Patterns." *Engineering Fracture Mechanics* 11(4): 621–33.

Sha, G et al. 2011. "Nanostructure of Aluminium Alloy 2024 : Segregation , Clustering and Precipitation Processes." *Acta Materialia* 59: 1659–70.

Stoychev, S., and D. Kujawski. 2003. "Methods for Crack Opening Load and Crack Tip Shielding Determination: A Review." *Fatigue and Fracture of Engineering Materials and Structures* 26(11): 1053–67.

Vasco-Olmo, J. M. et al. 2016. "Assessment of Crack Tip Plastic Zone Size and Shape and Its Influence on Crack Tip Shielding." *Fatigue and Fracture of Engineering Materials and Structures* 39(8): 969–81.

Vasco-Olmo, J M, F A Díaz, and E A Patterson. 2016. "Experimental Evaluation of Shielding Effect on Growing Fatigue Cracks under Overloads Using ESPI." *International Journal of Fatigue* 83(2): 117–26.

Walker, K. 1970. "The Effect of Stress Ratio During Crack Propagation and Fatigue for 2024-T3 and 7075-T6 Aluminum." *Effects of Environment and Complex Load History for Fatigue Life, STP 462, American Society for Testing and Materials* 1: 1–14.

Xia, Z., D. Kujawski, and F. Ellyin. 1996. "Effect of Mean Stress and Ratcheting Strain on Fatigue Life of Steel." *International Journal of Fatigue* 18(5): 335–41.